Supporting Information

Kidmose et al. 10.1073/pnas.1208031109

SI Materials and Methods

C4 and MASP-2 CCP1-CCP2-SP Purification. Purification was performed at 4–6 °C, and all columns were from GE Healthcare. Thawed citrated human plasma was made 10 mM in benzamidine (BZA), 3 μg/mL in pancreatic trypsin inhibitor, 60 mM in $BaCl_2$, and 25 mM in trisodium citrate. After centrifugation, the supernatant was loaded on a Q-Sepharose FF column equilibrated in 10 mM Tris·HCl, pH 7.5, 100 mM NaCl, 50 mM ε-Amino-Caproic Acid, 5 mM EDTA, 0.5 mM phenylmethylsulfonylfluoride (PMSF), and 1 mM BZA. Bound protein was eluted with a 100–500 mM NaCl gradient. To C4 containing fractions were added PEG6000 to a final concentration of 12% (wt/wt). After centrifugation, the pellet was redissolved in 200 mM NaCl, 20 mM Tris·HCl, pH 7.5, 1 mM BZA, and 0.5 mM PMSF and loaded on a Q-Sepharose HR column equilibrated in the same buffer and eluted with a 200- to 800-mM NaCl gradient. C4 containing fractions were diluted with water before loading on a Source 15Q column equilibrated in 100 mM NaCl, 20 mM Tris·HCl, pH 7.5, and 1 mM BZA and eluted with a 200- to 800-mM NaCl gradient. Pooled fractions were dialyzed against 20 mM Hepes, pH 7.7, and 100 mM NaCl. Recombinant MASP-2 CCP1–CCP2–SP S633A was prepared as described (1). The refolded protein was loaded on a Source 30Q column, washed with 50 mM NaCl, and eluted with a 100- to 400-mM NaCl gradient in 10 mM Tris·HCl, pH 8.2, and 1 mM EDTA. Zymogen MASP-2 was cleaved with recombinant MASP-1 CCP1–CCP2–SP (2, 3) by using 5 μg/mL MASP-1 and 100 μg/mL MASP-2 in 180 mM NaCl, 10 mM Tris·HCl, pH 8.2, and 1 mM EDTA. After cleavage, it was loaded on a Source 15S column and eluted with a 50- to 250-mM NaCl gradient in 10 mM Na–phosphate, pH 6.8. Cleaved MASP-2 was dialyzed against 300 mM NaCl, 5 mM Tris·HCl, pH 8.5, and 0.5 mM EDTA.

Structure Determination, Analysis, and Modeling. To crystallize the enzyme–substrate complex, C4 (15 mg/mL) was mixed with CCP1–CCP2–SP MASP-2 S633A (2.9 mg/mL) in a 1:1 molar ratio. Crystallization was performed by mixing equal volumes of premixed C4·MASP-2 complex and reservoir [100 mM Tris·HCl, pH 8.0, 2% (vol/vol) 1,4-dioxane, and 12–14% (wt/vol) PEG 3350]. Before flash freezing, crystals were gradually transferred to 25% (wt/vol) PEG 3350 and 15% (vol/vol) glycerol. To crystallize C4, it was concentrated to 6 mg/mL and mixed with an equal volume of reservoir [0.9 M sodium citrate, pH 6.4, 0.25 M potassium chloride, 1% (vol/vol) ethanol, 3% (vol/vol) acetonitrile, 6% (vol/vol) ethylene glycol, and 10 mM spermidine] at 19 °C. Crystals were transferred to a solution containing 37.5% (vol/vol) PEG 400, 50 mM MesNaOH, pH 6.4, 0.25 M KCl, 1% (vol/vol) ethanol, 3% (vol/vol) acetonitrile, 6% (vol/vol) ethylene glycol, and 10 mM trimethyllead acetate before flash freezing. The latter increased resolution and decreased anisotropy, but no sites were identified. For the Ta_6Br_{12} derivative, the compound was resuspended in reservoir solution and added to the crystals for soaking. Before flash freezing these crystals were briefly transferred to 0.9 M sodium citrate, pH 6.4, and 30% (vol/vol) glycerol. Diffraction data collected at European Synchrotron Radiation Facility (ESRF) ID29 or SOLEIL PROXIMA1 (Table S1) were processed with XDS (4) and molecular replacement carried out with PHASER (5). Rebuilding was done in O (6) after refinement of intermediate models with PHENIX.REFINE (7). A substantial improvement was obtained after combination of single-wavelength anomalous diffraction phases from the Ta_6Br_{12} derivative (figure of merit, 0.33; phasing power, 2.5) calculated with CNS (8) with model phases from PHENIX.REFINE followed by solvent flipping in CNS. Inclusion of the isomorphous differences between the C4–Ta_6Br_{12} data and the native C4 data in phasing did not improve the resulting density maps, probably due to significant differences in cell parameters (Table S1). Because the sequence identity between human C3 and C4 is 28%, several cycles of manual rebuilding and refinement were carried out, but the electron density for the MG3 and MG4 domains remained poorly defined. At R_{free} = 35% for the structure of unbound C4, the C4·MASP-2 diffraction data became available and molecular replacement with PHASER using the intermediate C4 model and the X-ray structure of activated MASP-2 (PDB ID code 1Q3X) as search models placed two copies of both C4 and MASP-2. From this point structure determination was promoted by the presence of two C4·MASP-2 complexes in the crystal, the known structure of active MASP-2 (9), and the ability to compare models of C4 either unbound or bound to MASP-2. In an averaged $2mF_o - DF_c$ density for the C4·MASP-2 complex generated with AVE (10) using individual domains of C4 or MASP-2 for averaging masks and generation of noncrystallographic symmetry (NCS) operators, the main chain of the MG3 and MG4 domains were easily traced. The C4 R-loop residues 750–761 were included in the mask for the MASP-2 SP domain, because these are interacting tightly. All subsequent rebuilding was done in such averaged electron densities, which could not be further improved by multiple crystal averaging using $2mF_o - DF_c$ or solvent-flattened densities resulting from the C4 and C4·MASP-2 structures. During refinement of C4·MASP-2, model restraints for MASP-2 derived from PDB ID code 1Q3X and restraints for parts of the C4 TE domain from the structure of C4Adg (PDB ID code 1HZF) were used together with tight NCS restraints applied domain-wise and secondary structure restraints as implemented in PHENIX.REFINE. Comparison with the C4·MASP-2 complex was also used to guide the iterative rebuilding of unbound C4, which was refined with secondary structure restraints in PHENIX.REFINE. For both structures translation/libration/screw (TLS) parameters were refined for the individual structural domains. The structures were refined with grouped B factors, but in the final refinement a few cycles of refinement with individual B factors were carried out as justified by a drop in R_{free}. Models were validated with PROCHECK (11) and MOLPROBITY (12). The final C4 structure had 78.1% of the residues (excluding proline and glycine) in favored regions of the Ramachandran plot, 21.6% in allowed regions, and 0.3% in disallowed regions. The equivalent statistics for the C4·MASP2 complex were 79.3%, 20.2%, and 0.5%. Molecular graphics figures were prepared with PYMOL (13). Sequence alignments were done with CLUSTALW (14).

C4 Deposition Assay. MASP-2 variants were generated from a MASP-2 expression plasmid (15) by site-directed mutagenesis (Quikchange II XL; Agilent Technologies). Plasmids were mixed with Lipofectamin-2000 and OptiPRO SFM (Invitrogen) and used for transfection of HEK293F cells (Invitrogen), according to the manufacturer's instructions. Cells were cultivated for 72 h in Freestyle 293 Expression Medium (Invitrogen), and the supernatants were harvested. FluoroNUNC plates were coated with mannan in 15 mM Na_2CO_3, 35 mM $NaHCO_3$, and 15 mM NaN_3, pH 9.6, and blocked with human serum albumin (HSA) in Tris-buffered saline [TBS; 10 mM Tris·HCl, 140 mM NaCl, pH 7.4 with 0.01% (wt/vol) NaN_3]. The wells were washed in TBS/Tw/Ca^{2+} [TBS with 0.05% (vol/vol) Tween-20 and 5 mM $CaCl_2$] and added 100 ng of rMBL (16) in 100 μL of TBS/Tw/Ca^{2+}. After 2 h at room temperature, the wells were washed, and to 12 wells were added 50 ng of WT MASP-2 or mutants in 100 μL of

TBS/Tw/Ca^{2+} and incubated overnight at 4 °C. The wells were washed, activation buffer (4 mM barbital, 145 mM NaCl, 2 mM $CaCl_2$, 1 mM $MgCl_2$, pH 7.4) was added, and they were incubated for 3 h at 37 °C. After wash, the wells were eluted with SDS/PAGE buffer [30 mM Tris·HCl, 10% (vol/vol) glycerol, 8 M urea, 3% (wt/vol) SDS, and 0.1% (wt/vol) bromophenol blue, pH 8.9] diluted 1:1 in TBS, and the eluate was analyzed by SDS/PAGE and Western blotting using an anti-MASP-2 antibody (1.3B7) (17). MASP-2 wild-type and mutant supernatants were analyzed without prior activation as above. The ability of the different MASP-2 variants to deposit C4 was tested as described (18). Mannan–MBL microtiter plate wells were generated as above, and dilutions of culture supernatant MASP-2 WT or mutants were added. After incubation overnight at 4 °C, the wells were washed and C4 was added, and after incubation for 1 h at 37 °C, the wells were developed by addition of biotinylated monoclonal anti-C4 antibody, followed by wash and addition of europium-labeled streptavidin. The amount of europium bound in the wells was measured by time-resolved fluorometry (Victor 3; Perkin-Elmer). The ability of the MASP-2 variants to mediate C4 deposition was also investigated in the presence of plasma. MASP-2–deficient plasma (15) was diluted to 1/200 in 1 M NaCl, 20 mM Tris·Base, 0.05% (vol/vol) Triton X-100, 10 mM $CaCl_2$, and 0.1% (wt/vol) HSA, pH 7.4; rMBL was added to 125 ng/mL, and rMASP-2 supernatant containing the MASP-2 variants was added. The mixtures were added to mannan-coated microtiter plate wells and tested for ability to C4 deposition as described above.

Inhibition of C1s by the C4 C345C Domain. DNA encoding C4 residues 1,591–1,744 and a cleavable His_6-tag (Genscript) was inserted in the pET32a(+) vector (Novagen). Mutations were made with the Quikchange Lightning Mutagenesis kit (Stratagene). Proteins were expressed in the *Escherichia coli* SHuffle T7 strain (New England Biolabs). Cells were resuspended in lysis buffer (50 mM Hepes·NaOH, pH 7.5, 300 mM NaCl, 30 mM imidazole·HCl, pH 7.6, and 1 mM PMSF), sonicated, and centrifuged, and the supernatant loaded on a HisTrap FF crude column. Bound proteins were eluted with 500 mM Imidazole·HCl. After digestion with tobacco etch virus–protease and dialysis against 20 mM Hepes·NaOH, pH 7.5, 300 mM NaCl, and 0.5 mM EDTA, untagged C345C was repurified on the HisTrap column and finally purified by size-exclusion chromatography on a Superdex 75 column equilibrated in 20 mM Hepes·NaOH, pH 7.5, and 200 mM NaCl. The C4 digests contained 0.025 μg/mL human C1s (Complement Technology; A104), 0.19 mg/mL C4, 25 mM Tris·HCl, pH 8.5, 10 mM glycine, 10 mM iodoacetamide, and 70 mM NaCl and were incubated at 37 °C for 30 min. If present, the C4 C345C domain variants were added in a molar ratio of 30:1 relative to C4. The intensities of the C4 β-and α′-chain bands were quantitated with TotalLab Quant v 11.4 (TotalLab Ltd).

Surface Plasmon Resonance (SPR) Studies. Measurements were performed by using a BIAcore 3000 instrument (GE Healthcare). The BIAcore CM5 sensor chip (GE Healthcare) was activated with a 1:1 mixture of 0.2 M *N*-ethyl-*N*′-(3-dimethylaminopropyl)carbodiimide and 0.05 M *N*-hydroxysuccimide in water. Before immobilization, proteins were diluted to 10 μg/mL in 10 mM sodium acetate, pH 4. Proteins were immobilized on the surface of the CM5 sensor chips at 0.0466 pmol/mm^2 (RU: 3460) for MASP-2 or 0.0779 pmol/mm^2 (RU: 5838) for C1s (Complement Technology; A104) in 150 mM NaCl, 3 mM EDTA, and 10 mM Hepes (pH 7.4) containing 0.005% surfactant P20 (GE Healthcare). Residual binding sites were blocked with 1 M ethanolamine, pH 8.5. Binding of equivalent concentrations of C4 345C WT, C4 345C R1724A, and C4 345C R1724E+T1721E was measured at a flow rate of 5 μL/min in 150 mM NaCl, 2 mM $CaCl_2$, 1 mM EGTA, and 10 mM Hepes (pH 7.4). The surface was regenerated by injections of 20 μL of 1.5 M NaCl. Equivalent volumes of each protein sample were injected over an activated and blocked reference surface without immobilized protein to provide blank sensorgrams for subtraction of the bulk refractive index background. SPR were analyzed by global fitting to a 1:1 Langmuir binding model of both the association and dissociation phases for four concentrations (80, 40, 20, and 10 nM) simultaneously by using the BIAevaluation 4.1 software (GE Healthcare). The apparent equilibrium dissociation constants (K_D) were calculated as the ratio of the dissociation and association rate constants (k_d/k_a).

1. Ambrus G, et al. (2003) Natural substrates and inhibitors of mannan-binding lectin-associated serine protease-1 and -2: A study on recombinant catalytic fragments. *J Immunol* 170:1374–1382.
2. Dobó J, et al. (2009) MASP-1, a promiscuous complement protease: Structure of its catalytic region reveals the basis of its broad specificity. *J Immunol* 183: 1207–1214.
3. Dobó J, et al. (2008) Purification, crystallization and preliminary X-ray analysis of human mannose-binding lectin-associated serine protease-1 (MASP-1) catalytic region. *Acta Crystallogr Sect F Struct Biol Cryst Commun* 64:781–784.
4. Kabsch W (2001) XDS. *International Tables for Crystallography*, Crystallography of Biological Macromolecules, eds Rossmann MG, Arnold E (Kluwer Academic, Dordrecht, The Netherlands), Vol F, pp 730–734.
5. McCoy AJ (2007) Solving structures of protein complexes by molecular replacement with Phaser. *Acta Crystallogr D Biol Crystallogr* 63:32–41.
6. Jones TA, Zou JY, Cowan SW, Kjeldgaard M (1991) Improved methods for building protein models in electron density maps and the location of errors in these models. *Acta Crystallogr A* 47:110–119.
7. Afonine PV, et al. (2012) Towards automated crystallographic structure refinement with *phenix.refine*. *Acta Crystallogr D Biol Crystallogr* 68:352–367.
8. Brünger AT, et al. (1998) Crystallography & NMR system: A new software suite for macromolecular structure determination. *Acta Crystallogr D Biol Crystallogr* 54: 905–921.
9. Harmat V, et al. (2004) The structure of MBL-associated serine protease-2 reveals that identical substrate specificities of C1s and MASP-2 are realized through different sets of enzyme-substrate interactions. *J Mol Biol* 342:1533–1546.
10. Kleywegt GJ, Read RJ (1997) Not your average density. *Structure* 5:1557–1569.
11. Laskowski RA, MacArthur MW, Moss D, Thornton JM (1993) PROCHECK: A program to check the stereochemical quality of protein structures. *J Appl Cryst* 26:283–291.
12. Lovell SC, et al. (2003) Structure validation by Calpha geometry: Phi, psi and Cbeta deviation. *Proteins* 50:437–450.
13. DeLano WL (2002) *The PyMOL User's Manual* (DeLano Scientific, San Carlos, CA).
14. Thompson JD, Higgins DG, Gibson TJ (1994) CLUSTAL W: Improving the sensitivity of progressive multiple sequence alignment through sequence weighting, position-specific gap penalties and weight matrix choice. *Nucleic Acids Res* 22:4673–4680.
15. Stengaard-Pedersen K, et al. (2003) Inherited deficiency of mannan-binding lectin-associated serine protease 2. *N Engl J Med* 349:554–560.
16. Jensenius JC, Jensen PH, McGuire K, Larsen JL, Thiel S (2003) Recombinant mannan-binding lectin (MBL) for therapy. *Biochem Soc Trans* 31:763–767.
17. Thiel S, et al. (2000) Interaction of C1q and mannan-binding lectin (MBL) with C1r, C1s, MBL-associated serine proteases 1 and 2, and the MBL-associated protein MAp19. *J Immunol* 165:878–887.
18. Thiel S, et al. (2009) Polymorphisms in mannan-binding lectin (MBL)-associated serine protease 2 affect stability, binding to MBL, and enzymatic activity. *J Immunol* 182: 2939–2947.

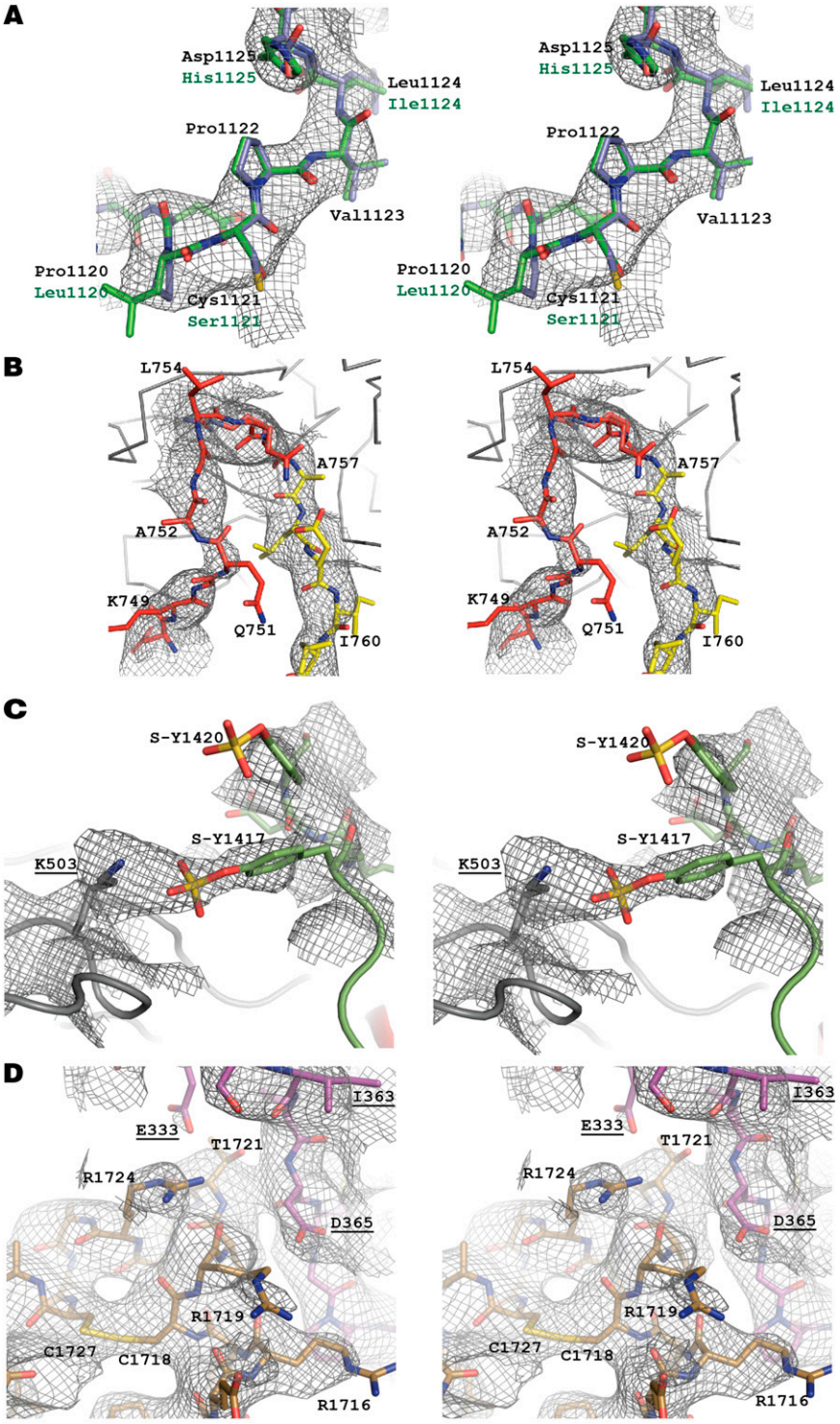

Fig. S1. Stereo representation of $2mF_o - DF_c$ electron densities from the C4·MASP-2 structure. MASP-2 labels are underlined. (*A*) Structures of C4·MASP-2 after refinement based on an input model with either the C4A sequence (blue carbon atoms, black labels) or the C4B sequence (green carbon atoms, green labels). The models are displayed together with an averaged omit $2mF_o - DF_c$ electron density contoured at 1σ calculated by omitting C4 residues 1,115–1,130. (*B*) Twofold averaged $2mF_o - DF_c$ electron density around the C4 R loop (red until Arg-756; yellow after) contoured at 1.2 σ. The MASP-2 SP domain (gray carbon atoms) is shown as a Cα trace. (*C*) Averaged omit $2mF_o - DF_c$ electron density around the sulfotyrosine region contoured at 1σ calculated by omitting C4 residues 1,417–1,420. In contrast to Y1417, the sulfo group on Y1420 does not form direct electrostatic interactions with any positive charge and is therefore likely to be free to rotate around the ester bond resulting in weak omit electron density. (*D*) The C4 C345C region (brown carbon atoms) recognized by the MASP-2 CCP exosite (magenta carbon atoms) in averaged $2mF_o - DF_c$ omit density contoured at 1σ. C4 residues 1,716–1,724 and MASP-2 residues 333–348, 364–365, and 416–417 were omitted for map calculation.

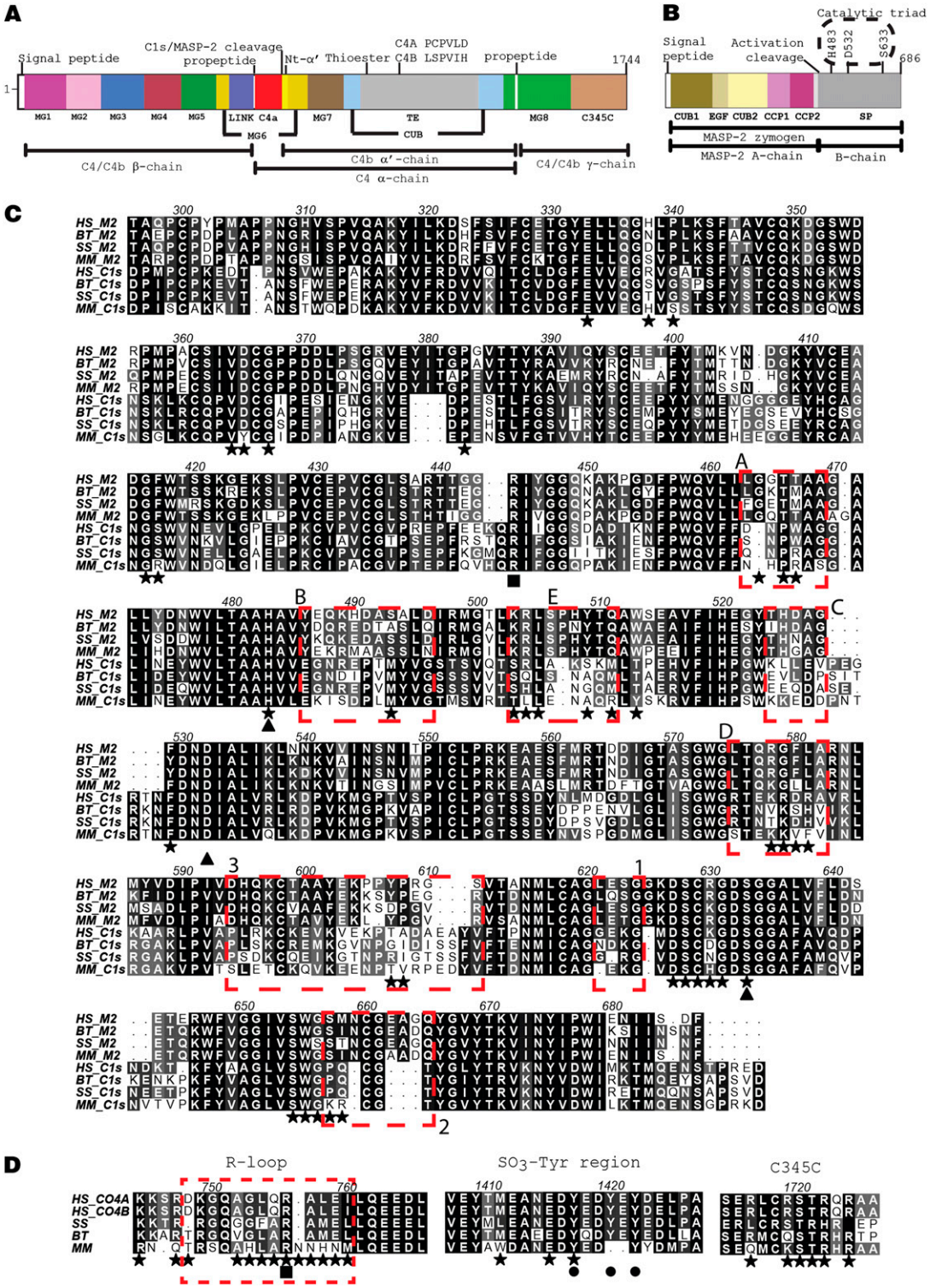

Fig. S2. Conservation of MASP-2 and C4 regions involved in intermolecular contacts. (*A*) Domain structure of C4 and definitions of the chains. Domains are colored as in Fig. 1*B*. (*B*) Domain structure of MASP-2 and the chain structure in zymogen and activated MASP-2. Domains are colored as in Fig. 1*C*. (*C*) Alignment of the CCP1–CCP2–SP region of selected mammalian MASP-2 and C1s sequences. ■, cleavage site for activation; ★, C4 contact, ▲, catalytic triad residue. Dashed squares indicate SP loop regions as defined by Perona and Craik (1) and applied to MASP-2 (2). (*D*) Alignment of regions involved in MASP-2 contacts in selected mammalian C4 sequences, residue numbering is according to human C4, for which both isoforms are shown. ■, C1s/MASP-2 cleavage site; ★, MASP-2 contact; ●, SO_3-tyrosine. In *A* and *B*, species abbreviations are as follows: HS, *Homo sapiens*; SS, *Sus scrofa* (pig); BT, *Bos taurus* (bovine); MM, *Mus musculus*. *C* and *D* were prepared with ALINE (3).

1. Perona JJ, Craik CS (1997) Evolutionary divergence of substrate specificity within the chymotrypsin-like serine protease fold. *J Biol Chem* 272:29987–29990.
2. Harmat V, et al. (2004) The structure of MBL-associated serine protease-2 reveals that identical substrate specificities of C1s and MASP-2 are realized through different sets of enzyme-substrate interactions. *J Mol Biol* 342:1533–1546.
3. Bond CS, Schüttelkopf AW (2009) ALINE: a WYSIWYG protein-sequence alignment editor for publication-quality alignments. *Acta Crystallogr D Biol Crystallogr* 65:510–512.

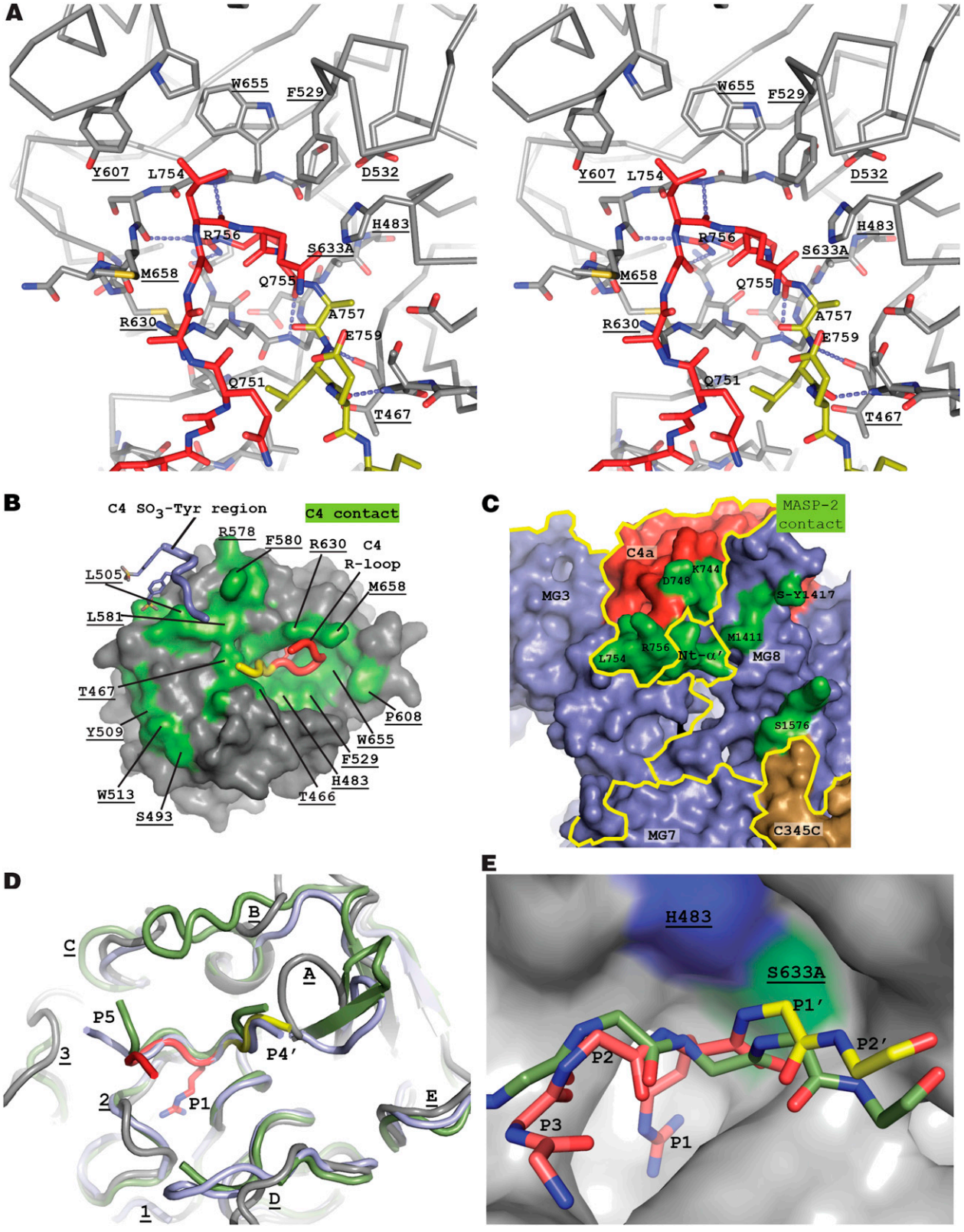

Fig. S3. Details of the R-loop interaction with MASP-2 and comparison of the R-loop main chain conformation to substrates of other SPs and a MASP-2 inhibitor. (*A*) Stereoview of the R loop (red carbon atoms until Arg-756; yellow after) bound to the MASP-2 SP domain (gray carbon atoms; labels underlined). (*B*) Footprint (MASP-2 residues within 3.8 Å of C4 shaded green) of C4 on the surface of the SP domain. (*C*) Footprint (green residues) of the MASP-2 SP domain on C4. *D* and *E* are related by a 180° rotation around a vertical axis. (*D*) Comparison of the overall path for the P5–P4′ region of the substrates in two SP·serpin complexes (light blue cartoon, PDB ID code 1K9O serpin 1B·trypsin (1); green cartoon, PDB ID code 1SR5 (2) antithrombin·anhydrothrombin·heparin complex) and in the C4·MASP-2 complex (MASP-2, gray cartoon; C4 R loop, red and yellow). The MASP-2 loop regions are labeled (underlined) according to ref. 3. (*E*)

Legend continued on following page

Peptide main-chain conformation of the substrate C4 (red-yellow carbon atoms) and the inhibitor SGMI_2 (4) (green carbons, PDB ID code 3TVJ) P3–P2′ region bound to MASP-2. The protease is shown as a gray surface illustrating the deep S1 pocket accommodating the P1 arginine. MASP-2 active site residues His-483 and Ser-633 (here mutated to alanine) are colored blue and green, respectively.

1. Ye S, et al. (2001) The structure of a Michaelis serpin-protease complex. *Nat Struct Biol* 8:979–983.
2. Dementiev A, Petitou M, Herbert JM, Gettins PG (2004) The ternary complex of antithrombin-anhydrothrombin-heparin reveals the basis of inhibitor specificity. *Nat Struct Mol Biol* 11: 863–867.
3. Harmat V, et al. (2004) The structure of MBL-associated serine protease-2 reveals that identical substrate specificities of C1s and MASP-2 are realized through different sets of enzyme-substrate interactions. *J Mol Biol* 342:1533–1546.
4. Héja D, et al. (2012) Monospecific inhibitors show that both mannan-binding lectin-associated serine protease-1 (MASP-1) and -2 are essential for lectin pathway activation and reveal structural plasticity of MASP-2. *J Biol Chem* 287:20290–20300.

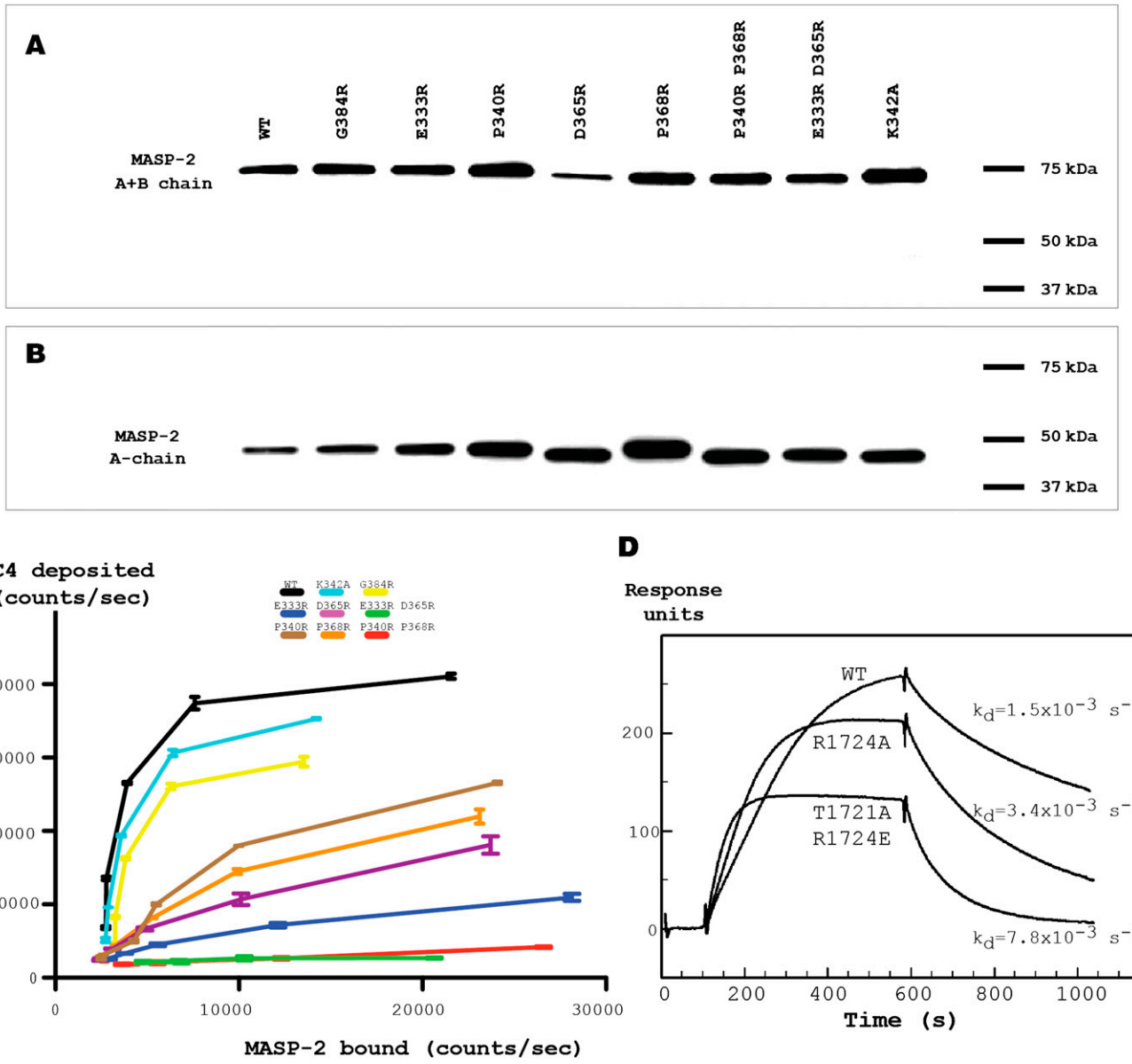

Fig. S4. The autoactivation and the activity of rMASP-2 variants. (*A*) Culture supernatants containing the various rMASP-2 variants (indicated above the lanes) were analyzed by SDS/PAGE under reducing conditions and Western blotting using an anti-MASP-2 antibody. (*B*) Recombinant MASP-2 containing supernatants were incubated in wells with rMBL bound to mannan, washed, and left at 37 °C. The wells were subsequently washed, and MBL and MASP-2 were eluted from the wells with SDS/PAGE sample buffer. The samples were then analyzed by SDS/PAGE at reducing conditions, followed by Western blotting developing with anti-MASP-2 antibody. The migration of the molecular mass markers is given on the right in kilodaltons. The position of the intact polypeptide chain (A+B in *A*) and the position of the A-chain seen after cleavage (*B*) are indicated on the left-hand side. When an MBL/MASP complex binds to an activating surface, pro-MASP-2 may autoactivate. When this happens, the polypeptide chain of MASP-2 is cleaved into two chains (the 52-kDa A and the 31-kDa B chain) held together by a disulfide bond. (*C*) The activity of the different MASP-2 variants in the presence of MASP-2 deficient plasma. rMBL and dilutions of rMASP-2 supernatants were added to MASP-2–deficient plasma, and the solutions were added to microtiter plate wells coated with mannan. After incubation and wash, C4 was added, and the wells were incubated and developed for C4 deposition as described. The result is depicted as for the experiment using purified component (Fig. 3*F*). (*D*) Assessment by SPR of the interaction between the C4 C345C domain and immobilized MASP-2. An overlay of sensorgrams representing 20 nM (close to the calculated K_D) of wild-type C4 C345C and two mutants is shown. Dissociation constants (K_D) are 20.7, 22.1, and 29 nM for WT C345C, C345C R1724A, and C345C T1721A,R1724E, respectively.

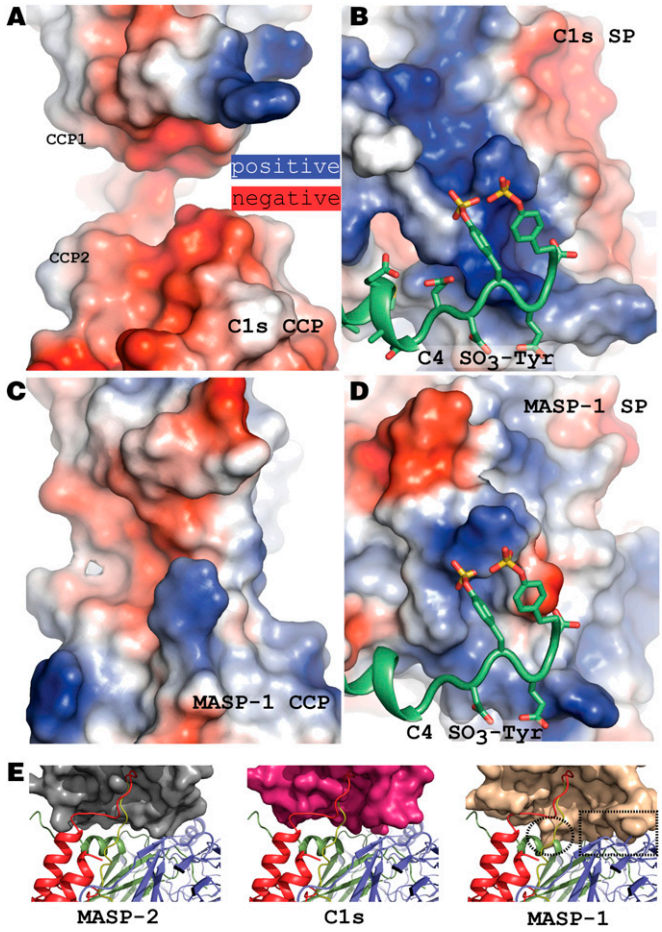

Fig. S5. Putative exosites in C1s for C4 binding and discrimination against C4 by MASP-1. (*A* and *B*) Surface electrostatic potential of a C1s model at the putative CCP exosite (*A*; same orientation as Fig. 3*E*) and the SP domain (*B*; same orientation as Fig. 2*D*). (*C* and *D*) As for *A* and *B*, but displaying MASP-1. (*E*) Comparison of the SP domains of MASP-2 (*Left*; gray surface), C1s (*Center*; pink surface), and MASP-1 (*Right*; wheat-colored surface). C4 is shown as a cartoon with the MG3 domain in blue, the C4a domain in red, the Nt-α′ region in yellow, and the MG8 domain in green. C1s and MASP-1 were docked onto MASP-2 through their SP domains. Although it seems plausible that C1s can bind C4 similar to MASP-2, MASP-1 apparently would be prevented from proper R-loop recognition due to major steric hindrance (dotted rectangle) exerted by the C4 MG3 domain and minor steric hindrance (dotted ellipse) exerted by the C4 MG8 domain.

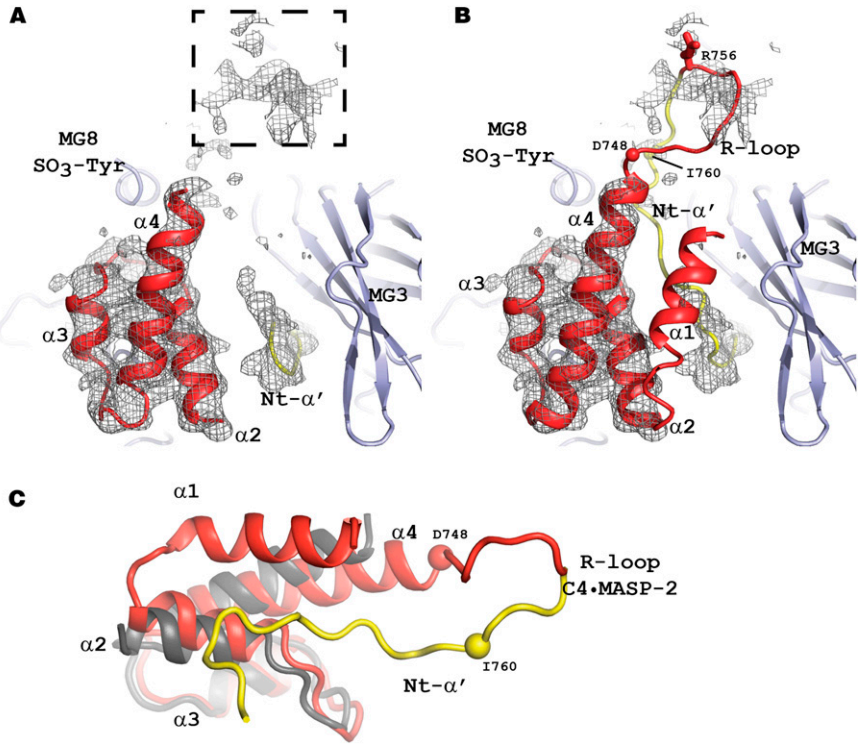

Fig. S6. Ordering and reorientation of C4a upon MASP-2 binding to C4. (*A*) The traceable parts of the C4a domain (red) and the Nt-α′ region (yellow) in $2mF_o - DF_c$ electron density contoured at 1σ from the structure of unbound C4. The dashed square indicates electron density for a symmetry-related molecule and can therefore not be attributed to the disordered R loop. (*B*) Same electron density but with C4a, R loop (red and yellow), and the Nt-α′ region from the C4·MASP-2 structure superimposed onto C4a from unbound C4, thereby for comparison showing where the untraceable regions—the α1-helix, the R loop, and part of the Nt-α′ region—are located in the C4·MASP-2 complex. (*C*) Comparison of the C4a (red), R loop (red-yellow), and Nt-α′ region (yellow) in C4·MASP-2 with the corresponding regions (gray) in unbound C4. Here, the structures of unbound C4 and C4·MASP-2 were superimposed on their α-chain superdomains to emphasize the relocation of C4a relative to α-chain superdomain upon MASP-2 binding.

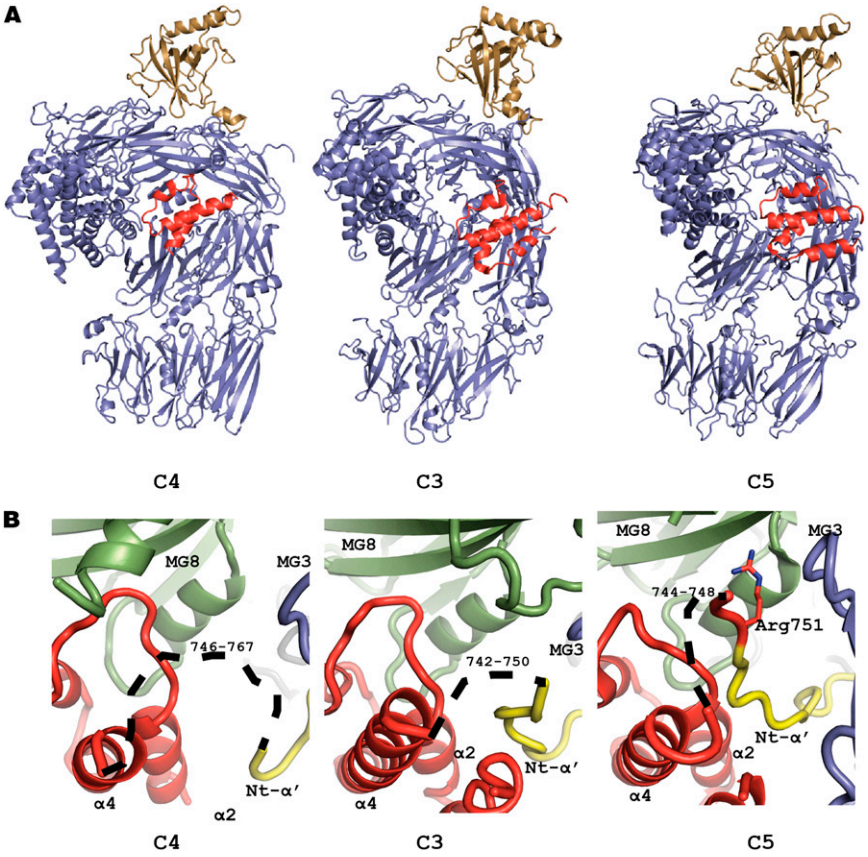

Fig. S7. Comparison of C3, C4, and C5. (*A*) Cartoon representation of the three paralogues emphasizing the high similarity in their overall 3D architecture. The three proteins [unbound C3 (1) and C4, CVF-bound C5 (2)] were superimposed on their MG1 and MG5 domains to obtain a common orientation. The anaphylatoxin domains are colored red, and the C345C domain is brown. (*B*) SP view of the scissile bond region in unbound human C4, C3 (1), and C5 (3). Cleavage of the scissile bond causes formation of the two products, the anaphylatoxins (C3a, C4a, or C5a) and the nascent large fragment (C3b, C4b, or C5b). The dotted line represents the mobile region (residue numbers indicated) connecting the α4-helix with the Nt-α′ region. In C5 the P1 residue Arg-751 is ordered. The proteins were superimposed on the α2-, α3-, and α4-helices of their anaphylatoxins.

1. Janssen BJ, et al. (2005) Structures of complement component C3 provide insights into the function and evolution of immunity. *Nature* 437:505–511.
2. Laursen NS, et al. (2011) Substrate recognition by complement convertases revealed in the C5-cobra venom factor complex. *EMBO J* 30:606–616.
3. Fredslund F, et al. (2008) Structure of and influence of a tick complement inhibitor on human complement component 5. *Nat Immunol* 9:753–760.

Table S1. Statistics for data collection and refinement

	C4	C4 Ta_6Br_{12}	C4·MASP-2
Data collection			
Beamline	ESRF ID29	SOLEIL Proxima 1	ESRF ID29
Space group	$P2_12_12_1$	$P2_12_12_1$	$P2_1$
a, *b*, *c*, Å	85.5, 103.3, 256.0	87.0,106.8,258.1	99.0,215.0,142.8
β,°			110.1
Resolution, Å	45.89–3.60 (3.73–3.60)	44.82–6.00 (6.24–6.00)	48.98–3.75 (3.86–3.75)
R_{sym}	9.7 (75.9)	9.4 (62.3)	11.6 (58.4)
$I/\sigma I$	13.2 (2.64)	10.72 (2.40)	9.45 (1.99)
Completeness, %	99.6 (99.9)	99.5 (100.0)	98.4 (97.1)
Redundancy	4.61 (4.84)	5.45 (5.2)	3.92 (2.48)
Refinement			
Resolution, Å	45.89–3.6 (3.73–3.60)		48.98–3.75 (3.86–3.75)
No. Reflections	25,600/1348		56,608/1727
R_{work}/R_{free}	20.0/26.9 (27.0/35.3)		17.4/24.2 (27.4/33.4)
No. of atoms	12,794		32,218
rms deviations			
Bond lengths, Å/angles, °	0.005/1.117		0.006/1.126

$R_{sym} = (\Sigma_h\Sigma_i |I(h)_I - <I(h)>|/\Sigma_h\Sigma_i I(h)_i)$ for the intensity of reflection *h* measured *N* times. Values in brackets are for outer resolution shell. *R* factor = $(\Sigma_h \mid |F_o| - k|F_c| \mid /\Sigma_h |F_o|)$ where F_o and F_c are the observed and calculated structure factor respectively, and *k* is a scaling factor. R_{free} factor is identical to the *R* factor on a subset of test reflections not used in refinement. One crystal was used for each dataset. Highest resolution shell is shown in parentheses.

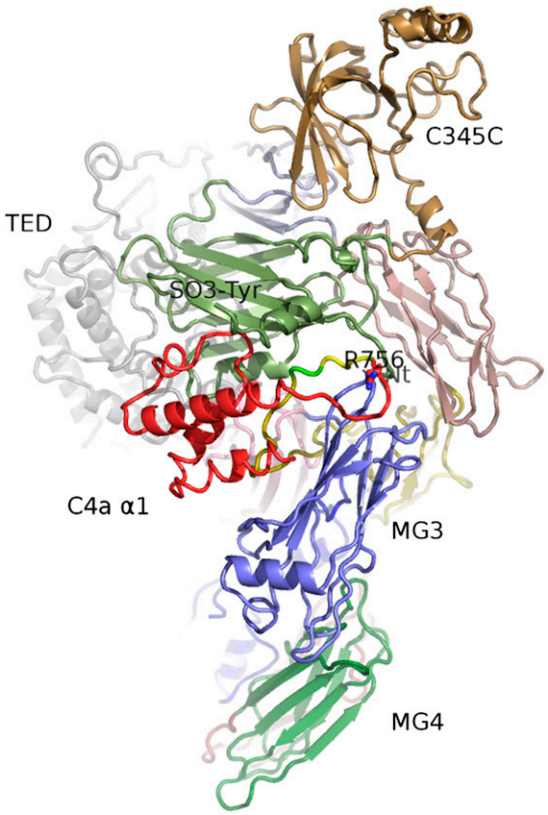

Movie S1. Conformational changes in C4 occurring upon MASP-2 binding. C4 is displayed with the domains colored as in Fig. 1*B*. To prepare the model of unbound C4 containing the same residues as C4 from the MASP-2 complex, which is required for interpolation between the two states, disordered residues in the C4a α1-helix, the R loop, and the sulfotyrosine region were modeled with O (1). These regions were placed merely to illustrate a conformational change upon MASP-2 binding, and their location is not built on experimental evidence. For the C4a α1-helix (residues 681–696) disordered in unbound C4, we fitted the C5a-desArg structure (PDB ID code 3HQA) onto C4a helices α2, α3, and α4. In this C5a structure, the α1 helix is ordered and exposed, but it does not interact with the remaining three helices. This location of the α1-helix is likely in the proforms of C3, C4, and C5 before cleavage between the β- and α-chain (2). We thereafter modeled the disordered C4a α1-helix after the exposed C5a α1-helix. A 30-state interpolation between the resulting modeled unbound C4 and C4 from the MASP-2 complex was conducted with the RIGIMOL option in PYMOL. The conformational changes shown here for the C4a α1 helix, the R loop, and the sulfotyrosine region are not built on experimental evidence, but help to illustrate a transition from a mobile conformation in unbound C4 (R-loop and sulfotyrosine region modeled) to an ordered conformation in MASP-2 bound C4 (R loop and sulfotyrosine region observed in our C4·MASP-2 structure). During the movie, C4 repeatedly shifts between the partially modeled unbound C4 conformation with the C4a α1-helix exposed, and the MASP-2 bound C4 conformation with the C4a α1-helix inserted between the MG3 domain (blue) and the rest of the C4a domain (red). Notice how the rotation of the C4 C345C domain (top) is transmitted through the MG7 and MG6 to the MG1-5 domains (bottom).

Movie S1

1. Jones TA, Zou JY, Cowan SW, Kjeldgaard M (1991) Improved methods for building protein models in electron density maps and the location of errors in these models. *Acta Crystallogr A* 47:110–119.
2. Cook WJ, Galakatos N, Boyar WC, Walter RL, Ealick SE (2010) Structure of human desArg-C5a. *Acta Crystallogr D Biol Crystallogr* 66:190–197.